

PCCP

Accepted Manuscript



This is an *Accepted Manuscript*, which has been through the Royal Society of Chemistry peer review process and has been accepted for publication.

Accepted Manuscripts are published online shortly after acceptance, before technical editing, formatting and proof reading. Using this free service, authors can make their results available to the community, in citable form, before we publish the edited article. We will replace this *Accepted Manuscript* with the edited and formatted *Advance Article* as soon as it is available.

You can find more information about *Accepted Manuscripts* in the [Information for Authors](#).

Please note that technical editing may introduce minor changes to the text and/or graphics, which may alter content. The journal's standard [Terms & Conditions](#) and the [Ethical guidelines](#) still apply. In no event shall the Royal Society of Chemistry be held responsible for any errors or omissions in this *Accepted Manuscript* or any consequences arising from the use of any information it contains.

Shock Wave Study and Theoretical Modeling of the Thermal Decomposition of c-C₄F₈

C. J. Cobos^a, K. Hintzer^b, L. Sölter^c, E. Tellbach^c, A. Thaler^b, and J. Troe^{c,d,*}

Submitted August 2015

Revised October 2015

to be published in Phys. Chem. Chem. Phys.

-
- a) INIFTA, Facultad de Ciencias Exactas, Universidad Nacional de La Plata, Argentina
 - b) Dyneon GmbH, Gendorf, D-84508 Burgkirchen, Germany
 - c) Institut für Physikalische Chemie, Universität Göttingen, Tammannstr. 6,
D-37077 Göttingen, Germany
 - d) Max-Planck-Institut für biophysikalische Chemie, Am Fassberg 11,
D-37077 Göttingen, Germany

*) jtroe@gwdg.de

Abstract

The thermal dissociation of octafluorocyclobutane, *c*-C₄F₈, was studied in shock waves over the range 1150 – 2300 K by recording UV absorption signals of CF₂. It was found that the primary reaction nearly exclusively produces 2 C₂F₄ which afterwards decomposes to 4 CF₂. A primary reaction leading to CF₂ + C₃F₆ is not detected (an upper limit to the yield of the latter channel was found to be about 10 percent). The temperature range of earlier single pulse shock wave experiments was extended. The reaction was shown to be close to its high pressure limit. Combining high and low temperature results leads to a rate constant for the primary dissociation of $k_1 = 10^{15.97} \exp(-310.5 \text{ kJ mol}^{-1}/RT)$ s⁻¹ in the range 630 – 1330 K, over which k_1 varies over nearly 14 orders of magnitude. Calculations of the energetics of the reaction pathway and the rate constants support the conclusions from the experiments. Also they shed light on the role of the 1,4-biradical CF₂CF₂CF₂CF₂ as an intermediate of the reaction.

Introduction

Octafluorocyclobutane, $c\text{-C}_4\text{F}_8$, is an important intermediate in the thermolysis of tetrafluoroethene, C_2F_4 , thus constituting evidence for a chain elongation during this process^{1,2}. Besides $c\text{-C}_4\text{F}_8$, substantial quantities of $\text{CF}_3\text{CF}=\text{CF}_2$, C_3F_6 , and $\text{CF}_2=\text{C}(\text{CF}_3)_2$, $i\text{-C}_4\text{F}_8$, have been observed earlier in this interesting reaction system. While it is well established that singlet difluorocarbene, CF_2 , plays an important role in the kinetics, it remains unclear whether C_3F_6 is a primary product of the decomposition of $c\text{-C}_4\text{F}_8$ or whether it arises from secondary interaction of CF_2 with C_2F_4 . A direct observation of CF_2 formation during the thermal dissociation of $c\text{-C}_4\text{F}_8$ may answer this question. This is the object of the present study. As CF_2 plays an important role in many technical applications, such as plasma etching with fluorocarbons, synthesis of fluorocarbon polymers and their incineration, understanding its reactions is of practical and fundamental interest as well.

In previous work we have investigated the temperature dependence of the UV absorption spectrum of CF_2 and carefully calibrated its absorption coefficient³. This gave us the opportunity to monitor the primary steps of the dissociations of C_2F_4 ³, C_3F_6 ⁴, and $c\text{-C}_3\text{F}_6$ ⁵ with respect to their rates and branching pathways. In continuation of these studies we now try to distinguish between the two primary dissociation pathways of $c\text{-C}_4\text{F}_8$,



and



where reaction (1) would be followed by



Beside reaction (2), C_3F_6 could also be formed by bimolecular processes like



While all previous studies⁶⁻¹³ used end product analysis and, in consequence, no direct observation of CF_2 was possible, it was difficult to unambiguously identify the origin of C_3F_6 . By studying the reaction in shock waves, one has the added benefit that wall reactions are excluded. The latter played some role in earlier low temperature experiments using static reactors (see the discussion by Poutsma¹). They were avoided in previous shock wave experiments¹¹⁻¹³ which used the single pulse technique. However, there were considerable discrepancies in the results of these studies^{12,13} which were attributed to shock wave non-idealities¹³. Accounting for these, satisfactory consistency of the rate constants from static reactor studies (e.g., experiments by Butler⁶ over the range 633 – 833 K) and from single-pulse shock waves (experiments by Simmie et al¹³ over the range 1100 – 1265 K) was obtained.

Different opinions were expressed about the branching between reactions (1) and (2). Nearly equal values of the rate constants k_1 and k_2 at 1200 K were suggested by Bauer and

Javanovic². $k_2 \ll 0.1 k_1$ was on the other hand concluded from the end product analysis of the single pulse shock wave experiments of Simmie et al¹³. As a consequence of these opposing conclusions, the *c*-C₄F₈ decomposition can so far not serve as a “chemical thermometer” for high temperature reactors, such as proposed by Bauer and Javanovic². By observing CF₂ directly in the reaction, the present study allows one to settle the question of the branching between reactions (1) and (2).

One could verify the simplicity of the mechanism of reaction (1) followed by reaction (3) in various ways. As long as conditions are employed where $k_1 \approx k_3$, CF₂ appearance should be accelerated with time and governed both by k_1 and k_3 . When $k_1 \gg k_3$, CF₂ appearance should be immediate and completely governed by reaction (3). Studying the reaction at the same temperature in reflected waves (with $k_1 \approx k_3$) and in incident waves (with $k_1 \gg k_3$ because of the falloff of k_3 at lower pressures³), the two pathways of the kinetics should become distinguishable in the present type of experiments.

Besides experimental work quantum-chemical calculations may help to clarify the energetics and structures of possible intermediates of reactions (1) and (2). With these results dissociation rate constants could be calculated by applying unimolecular rate theory. An important aspect here is the contribution of a pathway involving a 1,4-biradical CF₂CF₂CF₂CF₂, in competition to more direct pathways. The analogy to the mechanism of the decomposition of *c*-C₃F₆, involving an intermediate 1,3-biradical CF₂CF₂CF₂, is obvious and also of interest⁵. Our present quantum-chemical calculations update and extend earlier work from Yokoyama et al¹⁴. While the precision of our rate constant calculations will still

leave something to be desired, the comparison of experiment and theory nevertheless should shed some light on the question of the relative importance of reactions (1) and (2).

Experimental Technique and Results

As described in detail in our earlier work³⁻⁵, we recorded UV absorption signals of CF₂ at 248 nm during the dissociation of c-C₄F₈ behind incident and reflected shock waves. In brief, we used an aluminum shock tube of 10 cm inner diameter with a low pressure section of 4.15 m and a high pressure section of 2.80 m length. The driver gas was hydrogen at pressures between 2 and 15 bar. The light source for UV absorption measurements was a Xenon high pressure arc lamp (Osram XBO 150 W); wavelengths were selected by a prism monochromator (Zeiss, MQ3) and signals were recorded with a photomultiplier (Hamamatsu E2420) transient recorder arrangement. Mixtures of the reactant and the bath gas were prepared in large mixing vessels before the experiments. The initial concentrations of c-C₄F₈ (purity > 99 %, from abcr) in Ar (purity > 99,9999 %, from Air Liquide) were varied between 80 and 1000 ppm. Temperatures between 1150 and 2300 K were applied for CF₂ yield measurements and [Ar] was varied between about 4×10^{-6} and 4×10^{-5} mol cm⁻³ (corresponding to pressures in the range 1 – 10 bar).

We illustrate our observations first by Fig. 1 where the formation of CF₂ is recorded behind a reflected shock wave at 1328 K. The two spikes are schlieren signals indicating the arrival of the incident and reflected shock waves at the observation window. The formation of CF₂ behind the reflected wave follows roughly an exponential time law; however, deviations from this behavior in the initial stage of the reaction are quite obvious.

In the following we focus on three details of the signals: the final CF_2 yields, the time dependence of the CF_2 signals at the beginning of the reaction, and the effective rate constants of CF_2 formation during the main period of the reaction.

First, we consider the CF_2 yields, observed when the signals reach a plateau during our observation time. Doing experiments with reaction mixtures of about 80, 500, and 1000 ppm $\text{c-C}_4\text{F}_8$ in Ar, obtained behind incident and reflected shock waves and over the range 1500 – 2300 K, yields of $Y_\infty = [\text{CF}_2]_{t=\infty} / [\text{c-C}_4\text{F}_8]_{t=0} = 4.0(\pm 0.4)$ were observed. Slightly lower values of Y_∞ (near to 3.6) for the lowest reactant concentrations of 80 ppm were most probably due to some loss of reactant by wall adsorption during the preparation of the reaction mixtures before the experiments. The reaction sequence (1) and (3) would correspond to a CF_2 yield $Y_\infty = 4.0$. As C_3F_6 dissociates much slower than $\text{c-C}_4\text{F}_8$, reaction (2) would lead to $Y_\infty = 1.0$ (at least this is true as long as the bimolecular reaction (4) does not take place). The yield measurements here clearly indicate that reaction (1) dominates over reaction (2), with k_1 estimated to be at least 10 times larger than k_2 .

Next, we consider the starting period of the reaction. Fig. 2 shows an example which confirms the conclusions drawn from the yield measurements. The initial slope of CF_2 formation is very small; it cannot be distinguished from zero such that no CF_2 formation from reaction (2) is detectable. The delayed appearance of CF_2 recognized in the figure, on the other hand, can be interpreted by the reaction sequence (1) and (3) with reaction (3) not being fast enough to produce 4 CF_2 from $\text{c-C}_4\text{F}_8$ instantaneously. The CF_2 -profile, for a reaction sequence (1) and (3), can be represented in analytical form. Integrating the kinetic equations of reactions (1) and (3) (neglecting reactions (2) and (4)) leads to

$$Y(t) = [CF_2]_t / [c - C_4F_8]_{t=0} = 4 \left\{ 1 - \left[\frac{k_3}{k_3 - k_1} \right] \exp(-k_1 t) + \left[\frac{k_1}{k_3 - k_1} \right] \exp(-k_3 t) \right\} \quad (5)$$

Depending on the ratio k_1/k_3 , two regimes are possible. For $k_1 \ll k_3$, one has

$$Y(t) \approx 4 [1 - \exp(-k_1 t)] \quad (6)$$

whereas, for $k_1 \gg k_3$, eq. (5) approaches

$$Y(t) \approx 4 [1 - \exp(-k_3 t)] \quad (7)$$

Delays in the appearance of CF_2 are observed when $k_1 \approx k_3$. At the same time the effective rate constants for the main period of CF_2 formation contain contributions from k_1 and k_3 . The observation of delayed appearances, like those illustrated in Fig. 1 and 2 for experiments in reflected waves, indicates that k_1 and k_3 here are of similar magnitude. A further test for the understanding of the kinetics is provided by the comparison of results obtained from incident and reflected waves at similar temperatures. Then the bath gas concentrations $[Ar]$ differ by almost one order of magnitude. While reaction (1) remains in its limiting high pressure range (see below), k_3 falls off markedly with decreasing pressure³. The ratio k_1/k_3 thus increases distinctly by changing from reflected to incident waves, such that the delayed appearances of CF_2 disappear and the rate law approaches eq. (8). Fig. 3 illustrates this with a signal recorded

behind an incident wave. The schlieren signal at the arrival of the incident wave somewhat obscures the absence of the initial stage of the reaction, but the formation of CF_2 with the rate law of eq. (8) and the known value³ of k_3 is quite definite. As a consequence of this observation, information on k_1 can only be derived from measurements behind reflected waves, from the evaluation of the initial stage as shown in Fig. 2 and from an analysis of the full CF_2 profiles as shown in Fig. 1. Besides evaluating eq. (6) for reactions (1) and (3), we have treated the complete kinetics of reactions (1) – (4) with $k_2 \leq 0.1 k_1$ and k_4 such as given below. Numerical solution of the kinetic equations showed that the influence of reactions (2) and (4) on $Y(t)$ remained always smaller than the scatter of the signals of Figs. 1 – 3.

Extracting k_1 from the CF_2 profiles behind reflected waves under the present conditions meets some difficulties. It cannot be done without using the values of k_3 . A quick estimate of $\tau_{1/2}$, i.e. the time when $Y(\tau_{1/2}) = 2.0$, is provided by the approximate relationship

$$\bar{k} \tau_{1/2} = 0.765(\pm 0.075) \quad (8)$$

which follows from numerical evaluation of eq. (5) where \bar{k} denotes $k_1 k_3 / (k_1 + k_3)$. Eq. (8) bridges the gap between eqs. (6) and (7). While the CF_2 yield measurements in the present work are straight-forward, deriving k_1 is more cumbersome and can only be done in a limited range where k_1 is of the same order as k_3 . We illustrate the problem in Fig. 4 where k_1 from Butler⁶ and Simmie et al¹³ is compared with k_3 (at two different bath gas concentrations) from our earlier work³. Modeling the falloff curve of reaction (1) confirms that this reaction in all previous studies (including the present one) was in its high pressure range. In contrast to

this, falloff effects in reaction (3) had to be accounted for. Fig. 4, therefore, shows k_3 for $[\text{Ar}] = 4 \times 10^{-5} \text{ mol cm}^{-3}$ (as employed here in reflected waves) and $4 \times 10^{-6} \text{ mol cm}^{-3}$ (as employed here in incident waves). The comparison of k_1 with k_3 in Fig. 4 indicates that k_3 falls below k_1 with increasing temperature and decreasing pressure. Therefore, k_1 was here accessible only in experiments with reflected shock waves and low temperatures. Fig. 4 includes the measured points from Simmie et al¹³ and selected results from the present work. The latter were obtained by evaluating the full CF_2 profiles and/or the initial appearance (when only incomplete decomposition was reached within our observation time, which was about 1.5 ms after which perturbations from the contact surface started to become observable). Because of the necessity to employ also values of k_3 , the present results are estimated to be only accurate to a factor of 2. However, they extend satisfactorily the measurements of Simmie et al¹³ towards higher temperatures. Combining the results of Simmie et al¹³ and the present work with the low temperature data of Butler⁶, over the range 630 – 1330 K leads to

$$\begin{aligned} k_1 &= 10^{15.97} \exp(-310.5 \text{ kJ mol}^{-1} / RT) \text{ s}^{-1} \\ &= 10^{15.97} \exp(-37340 \text{ K} / T) \text{ s}^{-1} \end{aligned} \quad (9)$$

The results of the present work differ markedly from the recommendations of Bauer and Javanovic². Here, rate constants $k_1 = 2.10 \times 10^{16} \exp(-37389 \text{ K}/T) \text{ s}^{-1}$ and $k_2 = 1.58 \times 10^{17} \exp(-40000 \text{ K}/T) \text{ s}^{-1}$ were proposed. This would make k_1 almost equal to k_2 at the temperatures of the present study. In addition, k_1 was predicted to be roughly a factor of 4 larger than the values measured in the present study. The reasons for these discrepancies must be found in the indirect analysis of the reaction mechanism employed by Bauer and Javanovic² under much less simple conditions than those employed here. As the present study observes directly

the primary dissociation in the absence of a more complicated mechanism of secondary processes, it should lead to more reliable results for k_1 and to safer conclusions on the magnitude of k_2 .

The question remains how C_3F_6 was formed in earlier work under different conditions. An obvious candidate for C_3F_6 formation is the bimolecular reaction (4) which would not take place at the low reactant concentrations of the present work. With $k_4 / \text{cm}^3 \text{ mol}^{-1} \text{ s}^{-1} \approx 2.1 \times 10^{11} \exp(-1263 \text{ K}/T) + 6.9 \times 10^{14} \exp(-2134 \text{ K}/T)$ from our earlier work⁴, even at the highest concentrations (1000 ppm in Ar) realized in our work, reaction (4) could always be neglected. This was not the case for the lower T and higher reactant concentrations of earlier experiments.

Quantum-Chemical and Kinetic Modeling of the Primary Dissociation Steps

In the following section, we try to reconcile our experimental conclusions on reactions (1) and (2) with quantum-chemical calculations of the energetics and structural parameters of their intermediates and transition states. The calculations were performed at the G4MP2 ab initio composite level¹⁵, using B3LYP/6-31G(2df,p) optimized geometries, harmonic vibrational frequencies (scaled by the factor 0.9854) and single-point post-Hartree-Fock ab initio calculations for enthalpies of formation at 0 K. All calculations used the Gaussian 09 software¹⁶. We note that the G4MP2 enthalpies of formation (at 0 K) of singlet CF_2 and C_2F_4 were obtained as -198.2 and -667.8 kJ mol^{-1} , being satisfactorily close to tabulated values of¹⁷ -191.73 and -671.91 kJ mol^{-1} , respectively.

High pressure rate constants $k_{1,\infty}$ and $k_{2,\infty}$ were determined by conventional transition state theory (TST). Low pressure rate constants $k_{1,0}$ and $k_{2,0}$ were calculated using standard unimolecular rate theory¹⁸ while intermediate falloff curves connecting k_0 and k_∞ were constructed following the simplified procedure of Troe and Ushakov^{19,20}.

In agreement with the calculations of Yokoyama et al¹⁴ and the discussions by Poutsma¹ we found that reaction (1) proceeds as a two-step process with intermediate formation of the 1,4-biradical $\text{CF}_2\text{CF}_2\text{CF}_2\text{CF}_2$, followed by break-up of the central C-C bond leading to 2 C_2F_4 . On the other hand, reaction (2) was found to involve a single transition state only. Fig. 6 shows a sketch of the corresponding energy diagram, whose values, however, somewhat differ from those by Poutsma, constructed on the basis of earlier kinetic and thermochemical information only. $\text{CF}_2\text{CF}_2\text{CF}_2\text{CF}_2$ was found to correspond to two loosely bound C_2F_4 molecules separated by a C-C bond distance of about 3.7 Å (a triplet $\text{CF}_2\text{CF}_2\text{CF}_2\text{CF}_2$ with C-C distance of 1.55 Å was also located at 46 kJ mol⁻¹ above the singlet ground state). The rate-determining energy barrier of reaction (1) was found to be that for forming $\text{CF}_2\text{CF}_2\text{CF}_2\text{CF}_2$ from *c*- C_4F_8 . The transition from $\text{CF}_2\text{CF}_2\text{CF}_2\text{CF}_2$ to 2 C_2F_4 was suggested to occur fast by simple bond scission. The long bond between two C_2F_4 in $\text{CF}_2\text{CF}_2\text{CF}_2\text{CF}_2$ is also the reason why reaction (2) does not involve the same biradical intermediate. Instead, it has its own transition state to form $\text{C}_3\text{F}_6 + \text{CF}_2$. The latter according to our calculations at somewhat higher energies than for reaction (1).

Structural parameters required for the calculations of $k_{1,0}$ and $k_{1,\infty}$, as calculated here for *c*- C_4F_8 and the two transition states, are given in the Appendix. Further parameters calculated are given in the Supplementary Material. Figs. 6 and 7 compare the structures of the two transition states. $k_{1,\infty}$ and $k_{2,\infty}$ can be estimated with the energies, frequencies and rotational constants given in the Appendix. However, there is some ambiguity about how the low-frequency torsions should be handled. A purely harmonic vibrational model would lead to $k_{1,\infty}$

$\approx 6.4 \cdot 10^{14} \exp(-39450 \text{ K}/T) \text{ s}^{-1}$ and $k_{2,\infty} \approx 1.7 \cdot 10^{14} \exp(-41920 \text{ K}/T) \text{ s}^{-1}$. While this leads to $k_{1,\infty}/k_{2,\infty} > 10$ at all temperatures of the present work, being in agreement with the conclusions from our experiments, it differs markedly from the earlier suggestion² of $k_{1,\infty} \approx k_{2,\infty}$.

Meanwhile, the calculated $k_{1,\infty}$ are lower than the measured values. Replacing the 90 cm^{-1} torsion of TS1 by a free rotation (with a reduced moment of inertia of 62 amu \AA^2), could partly cure the problem. One then obtains

$$k_{1,\infty} \approx 5.0 \cdot 10^{15} \exp(-38800 \text{ K}/T) \text{ s}^{-1} \quad (10)$$

which would be only a factor of 2-3 below eq. (9) from the measurements. The disagreement with the values from Bauer and Javanovic² on the other hand is more pronounced, being about a factor of ten. The remaining discrepancy between eqs. (9) and (10) may be due to the general uncertainties in the calculated TS energies from the used quantum-chemical methods. However, changing the two other low-frequency torsions of TS1 into hindered or free internal rotations (see their frequencies in the Appendix) could also raise the preexponential factor of eq. (10) towards the measured value of eq. (9). We did not further explore the barriers for hindered rotations of the three low frequency torsions of TS1. Instead, we conclude that the measured k_1 is at least semi-quantitatively consistent with the calculations. In addition, $k_1 \gg k_2$ is confirmed. We note that the conclusions about the two-step character of reaction (1) is also consistent with the molecular beam study of Yokoyama et al¹⁴, measuring the translational energy of the C_2F_4 fragments in the multiphoton dissociation of *c*- C_4F_8 .

In addition to calculations of $k_{1,\infty}$ and $k_{2,\infty}$ we have also constructed full falloff curves for reactions (1) and (2). We do not elaborate the results here because falloff corrections for both reactions were found to be negligible under all conditions considered. In order to be able to do the corresponding estimates, low pressure rate constants are given in the Appendix.

Conclusions

Although the quantitative agreement between measured and calculated k_1 is not perfect, several conclusions appear justified. The primary decomposition of *c*-C₄F₈ is quite clearly determined by formation of 2 C₂F₄ in a two-step process with the 1,4 biradical CF₂CF₂CF₂CF₂ as an intermediate. Our calculations indicate that the primary ring opening is rate determining, while the subsequent dissociation of the central bond by a simple bond scission is fast. This differs from the conclusions of Yokoyama et al¹⁴ who suggested that the latter process is rate determining. In agreement with their results, we find that the formation of CF₂ + C₃F₆ is a single-step process. However, due to its higher energy barrier it contributes only to a very minor extent to *c*-C₄F₈ decomposition. Our results suggest that the reaction product C₃F₆ in *c*-C₄F₈ decomposition is formed by secondary processes, for instance a reaction of CF₂ with C₂F₄ (4).

Appendix Molecular Parameters

Results from quantum-chemical calculations (see text):

Threshold energies for reactions (1) and (2): 318.4 kJmol⁻¹ (TS1) and 341.0 kJ mol⁻¹ (TS2), respectively.

Frequencies (in cm⁻¹): *c*-C₄F₈: 34, 175 (2), 177, 207, 244, 267, 272 (2), 341, 353, 430 (2), 556 (2), 591, 649, 694, 845, 956 (2), 976, 1206 (2), 1233, 1248, 1283, 1314 (2), 1414;

transition state TS1: 147i, 90, 100, 125, 156, 206, 212, 232, 260, 274, 324, 347, 370, 406, 470, 519, 585, 595, 622, 702, 860, 950, 1038, 1069, 1141, 1176, 1313, 1343, 1390, 1477;

transition state TS2: 656i, 66, 113, 172, 198, 200, 242, 250, 290, 309, 343, 353, 401, 432, 519, 571, 598, 637, 656, 682, 784, 870, 1048, 1124, 1171, 1224, 1306, 1346, 1440, 1446.

Rotational constants (in cm^{-1}): c-C₄F₈: 0.0354 (2), 0.0288; $\sigma = 4$. TS1: 0.0414, 0.0283, 0.0237; $\sigma = 1$. TS2: 0.0422, 0.0285, 0.0271; $\sigma = 1$.

Structures of the transition states TS1 and TS2 illustrated in Figs 7 and 8

Low pressure strong collision rate constants: $k_{1,0}/[\text{Ar}] \text{ cm}^3 \text{ mol}^{-1} \text{ s}^{-1} = 4.4 \cdot 10^{12}$, $1.0 \cdot 10^{14}$, $3.8 \cdot 10^{14}$, and $4.9 \cdot 10^{14}$; $k_{2,0}/[\text{Ar}] \text{ cm}^3 \text{ mol}^{-1} \text{ s}^{-1} = 1.5 \cdot 10^{11}$, $9.2 \cdot 10^{13}$, $4.2 \cdot 10^{14}$, and $6.0 \cdot 10^{14}$

for T/K = 1000, 1500, 2000, and 2500, respectively.

References

- (1) M. L. Poutsma, *J. Anal. Pyrol.*, *92*, 25 (2011).
- (2) S. H. Bauer and S. Javanovic, *Int. J. Chem. Kinet.*, *30*, 171, (1998).
- (3) C. J. Cobos, A. E. Croce, K. Luther, L. Sölter, E. Tellbach and J. Troe, *J. Phys. Chem. A*, *117*, 11420 (2013).
- (4) C. J. Cobos, L. Sölter, E. Tellbach and J. Troe, *J. Phys. Chem. A*, *188*, 4880 (2014).
- (5) C. J. Cobos, L. Sölter, E. Tellbach and J. Troe, *J. Phys. Chem. A*, *188*, 4873 (2014).
- (6) J. N. Butler, *J. Am. Chem. Soc.*, *84*, 1393 (1962).
- (7) B. Atkinson and V.A. Atkinson, *J. Chem. Soc.*, 2086 (1957).
- (8) B. Atkinson and A. B. Trenwith, *J. Chem. Phys.*, *20*, 754 (1952).
- (9) B. Atkinson and A. B. Trenwith, *J. Chem. Soc.*, 2082 (1953).
- (10) N. N. Buravtsev, A. S. Grigorev and Yu. A. Kolbanovskii, *Kinet. Cat.*, *26*, 7 (1985).
- (11) S. H. Bauer, K. C. Hou and E. L. Resler, *Phys. Fluids Supp 1*, *12*, 125 (1969).
- (12) A. Lifshitz, H. F. Carroll and S. H. Bauer, *J. Chem. Phys.*, *39*, 1661 (1963).
- (13) J. M. Simmie, W. J. Quiring and E. Tschuikow-Roux, *J. Phys. Chem.*, *73*, 3830 (1969).
- (14) A. Yokoyama, K. Yokoyama and G. Fujisawa, *Chem. Phys. Lett.*, *237*, 106 (1995).
- (15) L. A. Curtiss, P. C. Redfern and K. Raghavachari, *J. Chem- Phys.*, *127*, 124105 (2007).

- (16) M. J. Frisch et al, Gaussian 09, Revision A.02 – SMP (Gaussian, Inc., Wallingford, CT, **2009**).
- (17) E. Goos, A. Burcat and B. Ruscic, Extended Millenium Ideal Gas and Condensed Thermochemical Database for Combustion with Updates from Active Thermochemical Tables (Report ANL 05/20 and TAE 960 Technion-IIT, 2005)
- (18) J. Troe, *J. Phys.Chem.*, 83, 114 (**1979**).
- (19) J. Troe, *Ber. Bunsenges. Phys. Chem.*, 87, 161 (**1983**).
- (20) J. Troe and V. G. Ushakov, *Z. Phys. Chem*, 228, 1 (**2014**).

Figure Captions

Fig. 1 Formation of CF_2 from $\text{c-C}_2\text{F}_4$ behind reflected shock wave (CF_2 absorption at 248 nm, $T = 1328 \text{ K}$, $[\text{Ar}] = 4.2 \cdot 10^{-5} \text{ mol cm}^{-3}$, $[\text{c-C}_4\text{F}_8]/[\text{Ar}] = 535 \text{ ppm}$, $\text{OD}=1$ corresponds to $[\text{CF}_2] = 3.5 \cdot 10^{-8} \text{ mol cm}^{-3}$).

Fig. 2 As Fig. 1 ($T = 1184 \text{ K}$, $[\text{Ar}] = 4.8 \cdot 10^{-5} \text{ mol cm}^{-3}$, $[\text{c-C}_4\text{F}_8]/[\text{Ar}] = 1024 \text{ ppm}$, $\text{OD} = 1$ corresponds to $[\text{CF}_2] = 3.2 \cdot 10^{-8} \text{ mol cm}^{-3}$).

Fig. 3 Formation of CF_2 from $\text{c-C}_2\text{F}_4$ behind incident shock wave (CF_2 absorption at 248 nm, $T = 1547 \text{ K}$, $[\text{Ar}] = 5.4 \cdot 10^{-6} \text{ mol cm}^{-3}$, $[\text{c-C}_4\text{F}_8]/[\text{Ar}] = 1024 \text{ ppm}$, $\text{OD} = 1$ corresponds to $[\text{CF}_2] = 3.8 \cdot 10^{-8} \text{ mol cm}^{-3}$).

Fig. 4 Rate constants k_1 for $\text{c-C}_4\text{F}_8$ decomposition (full line = eq. (9) from this work, refs. 6 and 13; filled symbols = selected experimental results from this work, open symbols = experimental results from ref. 13) and rate constants k_3 for C_2F_4 decomposition from ref. 3 (dashed line = k_3 for $[\text{Ar}] = 4 \cdot 10^{-5} \text{ mol cm}^{-3}$, dotted line = k_3 for $[\text{Ar}] = 4 \cdot 10^{-6} \text{ mol cm}^{-3}$).

Fig. 5 Schematic energy diagram for two dissociation possibilities of $\text{c-C}_4\text{F}_8$ (energies in kJ mol^{-1} from the present quantum-chemical calculations, see text).

Fig. 6 Quantum-chemically calculated structure of transition state TS1 (see Fig. 5; distances in 10^{-8} cm , angles in degrees).

Fig. 7 Quantum-chemically calculated structure of transition state TS2 (see Fig. 5; distances in 10^{-8} cm , angles in degrees).

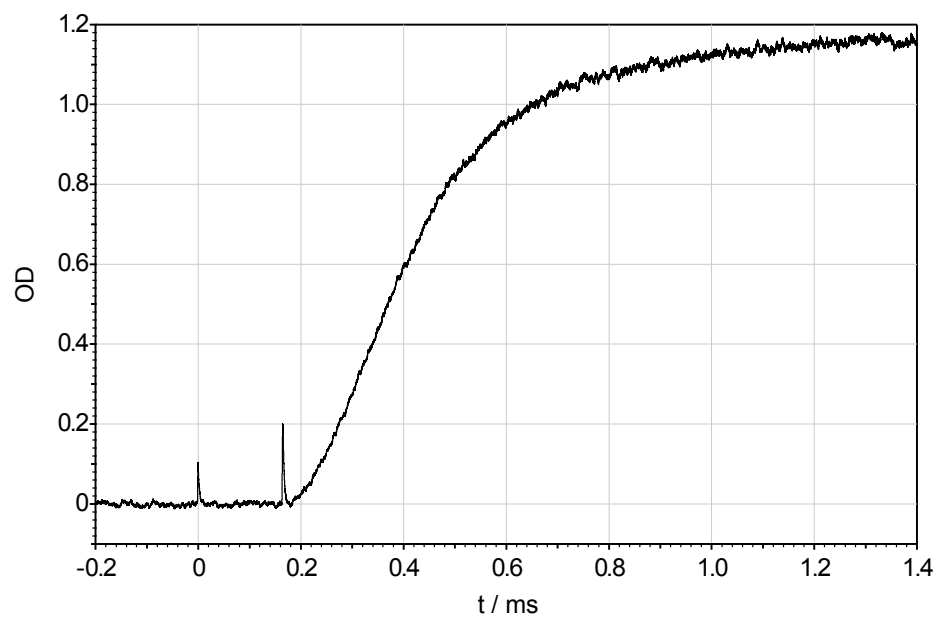


Fig. 1

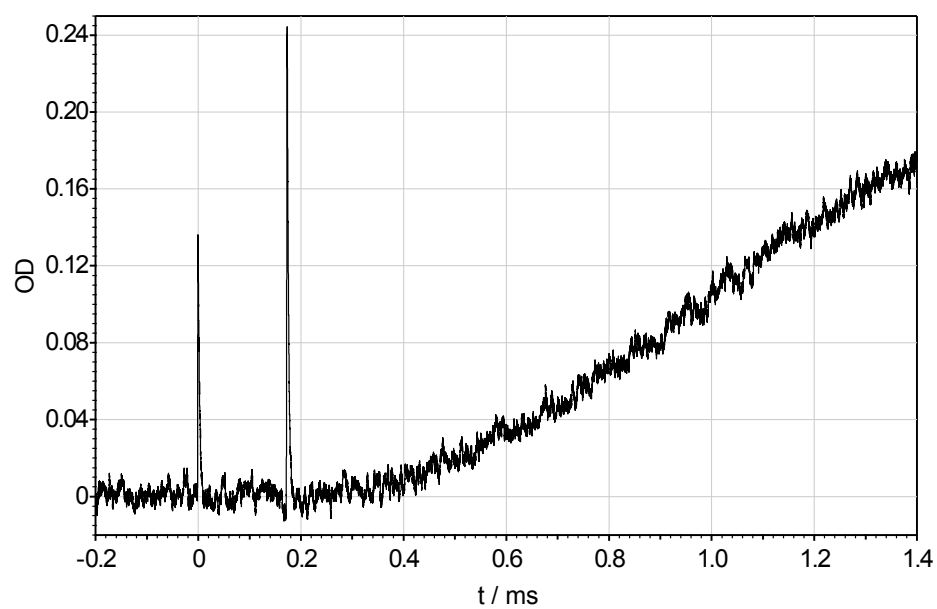


Fig. 2

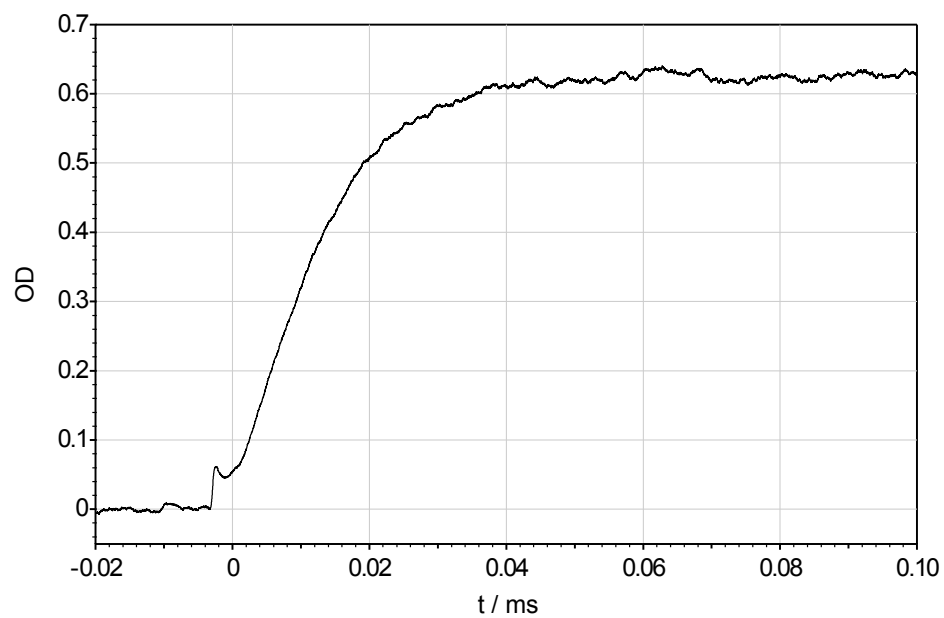


Fig. 3

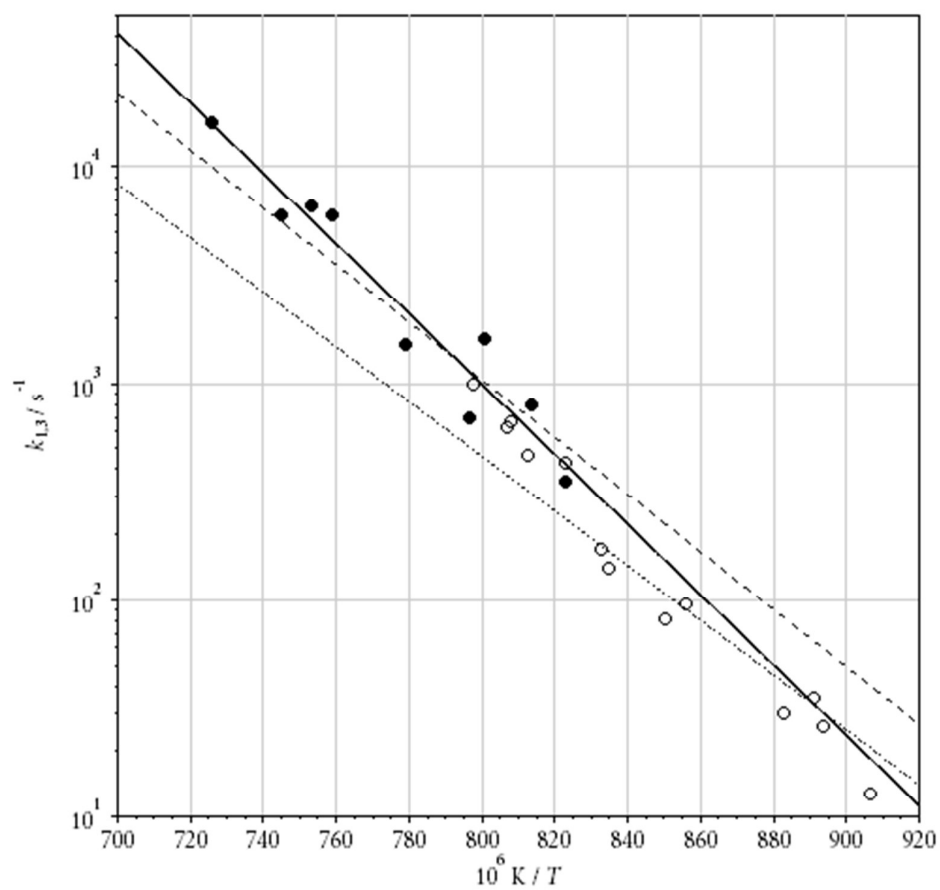


Fig. 4

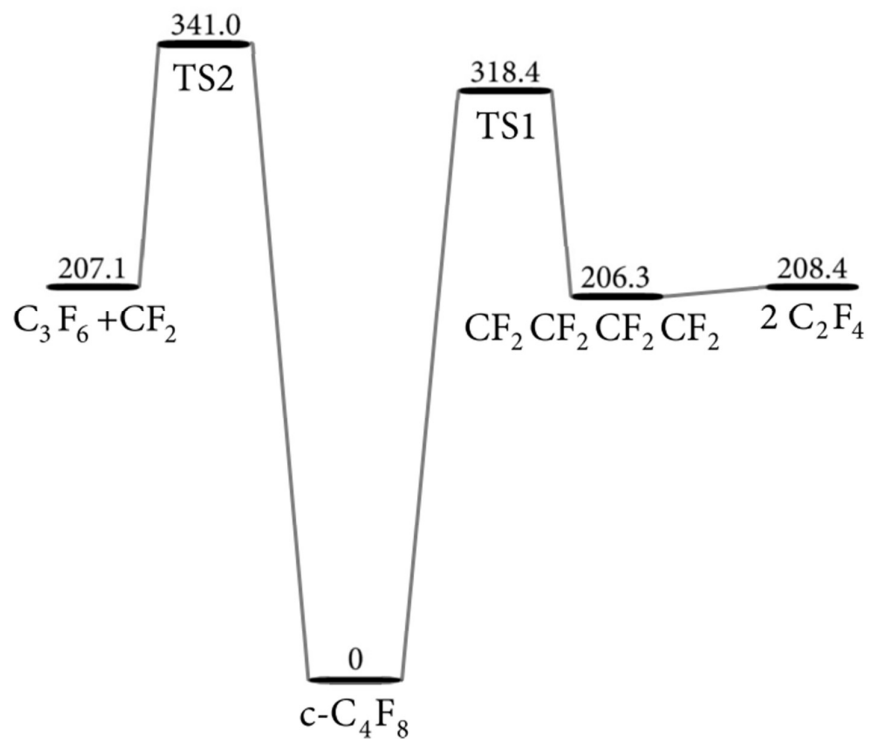


Fig. 5

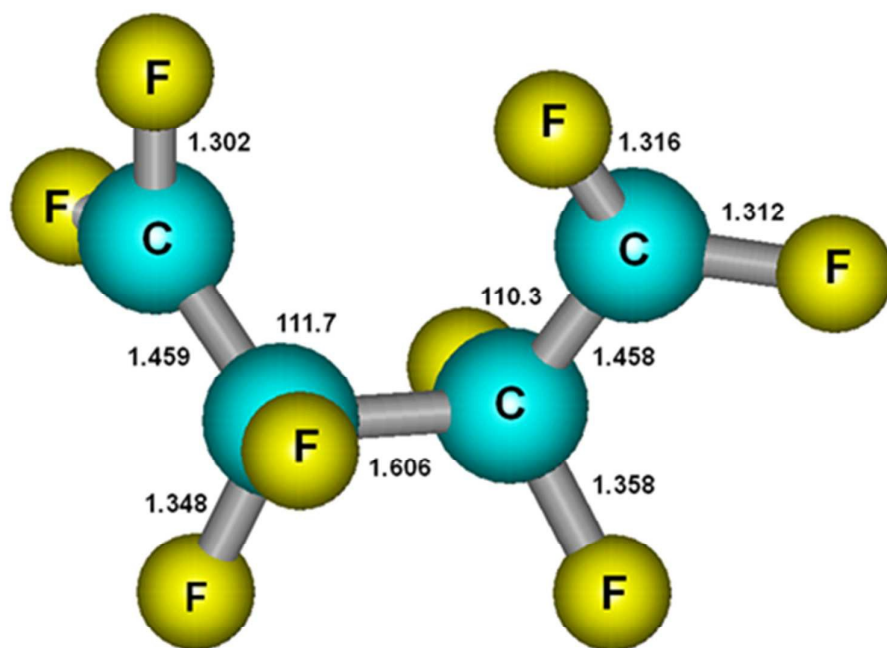


Fig. 6

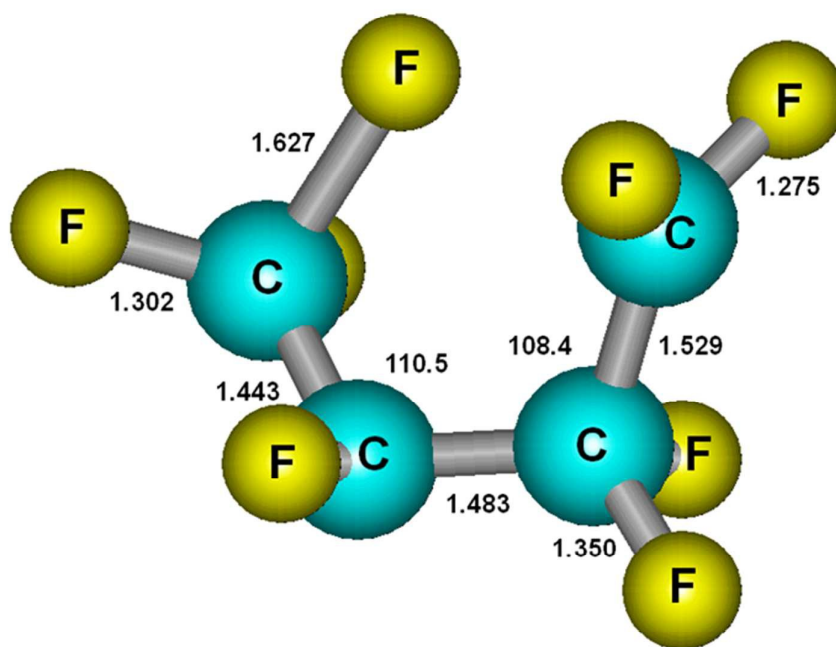


Fig. 7